Nanoscale

Photoswitchable Fluorescent Nanoparticles and Their Emerging Applications

Journal:	*Nanoscale*
Manuscript ID	NR-REV-08-2015-005436.R1
Article Type:	Review Article
Date Submitted by the Author:	09-Sep-2015
Complete List of Authors:	Zhang, Yuanlin; Key Laboratory for Special Functional Materials of the Ministry of Education, Henan University Zhang, Kaiquan; University of Chinese Academy of Sciences, School of Chemistry and Chemical Engineering Wang, Jie; University of Chinese Academy of Sciences, School of chemistry and Chemical Engineering Tian, Zhiyuan; University of Chinese Academy of Sciences, School of chemistry and Chemical Engineering Li, Alexander; Washington State University, Chemistry

Photoswitchable Fluorescent Nanoparticles and Their Emerging Applications

Yuanli Zhang[a], Kaiquan Zhang[a], Jie Wang[a], Zhiyuan Tian*[a], Alexander D. Q. Li*[b]

[a]School of Chemistry and Chemical Engineering, University of Chinese Academy of Sciences (UCAS), Beijing 100049, P. R. China,
[b]Department of Chemistry and Center for Materials Research, Washington State University, Pullman, Washington 99164, United States
zytian@ucas.ac.cn; dequan@wsu.edu

1. Introduction

Smart materials that respond to external stimuli have attracted ever-increasing attention because they can be applied to various emerging fields such as optoelectronic logic devices, ultrahigh density optical data storage, biological and biomedical imaging for exploring information regarding biological processes or mechanisms within cells, tissues or animals. [1-6] Among different forms of stimulus-induced signal modulation, fluorescence is particularly promising because fluorescence offers not only ultrahigh sensitivity but also self-identifying characteristics such as emission maximum, emission color, and signal lifetime. [7] Light, as an external stimulus that can modulate the selected property of a dynamic material, can be manipulated easily and delivered with precise spatiotemporal control. Moreover, it requires no physical contact and thus avoiding potential risk of chemical contamination.[8-14] More importantly, the selected property in a dynamic material responds to a specific region of light wavelengths is of significance as this provides orthogonality and multiplexing. This makes light-triggered modulation of selected properties unique when compared to other types of stimuli-responsive modes. For example, dynamic materials with modulatable magnetization features that respond to light stimulation have great potential applications in display and devices for storing information and energy. [15, 16]

Because fluorescent molecules ubiquitously exist in nature, for instance cell autofluorescence, precise identification of biological targets and ambiguous separation of signals from interference in biological tissues and other complex

specimens represent daunting challenges in fluorescence-based biological detection and biomedical diagnosis. Moreover, the intrinsic opacity and heterogeneity of the biological samples can mask the tag signals of even the highest fluorescence quantum yield, which make it difficult to distinguish the labeled targets from background, particularly in the case of a target at low concentrations. [17]

Despite widespread use of fluorescence for non-invasive imaging has provided a wealth of information regarding various biological mechanisms, the limit of classical optical diffraction, typically ~250 nm, restricts the best resolution of conventional fluorescence imaging to a level enormously coarser than the nanometer scale of biological structures and therefore renders many intracellular targets unaddressable. Thus, innovative fluorescence-based detection strategies to circumvent the aforementioned limitation of the conventional techniques are critically needed, particularly those that are capable of detecting low-copy-number targets in the presence of large noises or interferences and intelligently circumventing the diffraction limit barrier. Recently, photodynamic materials with modulatory fluorescence in response to external light stimuli, namely photoswitchable, photoconvertible, or photoactivatable fluorophores, have been successfully applied in fluorescence-based detections, which dramatically circumvent the long-standing impediments usually encountered in the conventional fluorescence analytical methods. For instance, the revolutionary role of molecular probes possessing photoswitchable fluorescence in wide-field super-resolution fluorescence imaging has already been demonstrated, which dramatically enables visualizing subcellular features with the nanoscale spatial resolution, far beyond the diffraction limit. [18-22]

Single-molecule fluorophores and genetically encoded fluorescent proteins with photomodulatable fluorescence have been used for distinguishing target signals from background noises and super-resolution imaging. Single-molecule photoswitchable fluorophores are typically characterized by their simple structures and relatively small physical size, which are expected to minimize the potential perturbation that exogenous probes may impart to biological systems such as live cells and tissue. Because fluorescent proteins can be genetically engineered to fuse with target proteins,

the combined protein typically retains biological activities and reports its location via the fluorescent protein, eliminating the need for specific labeling of the exogenous probes. However, the low photobleaching thresholds make single-molecule fluorophores and fluorescent proteins more vulnerable to light illumination-a critical drawback for long-term imaging applications such as tracking experiments involving live cells and tissue. It is also noted that in the case of using single-molecule fluorophores and fluorescent proteins as labeling reagents, limited fluorescence brightness per labeled site greatly hinder improvement in fluorescence detection sensitivity and imaging resolution.

In contrast, fluorescent nanoparticles (NPs) offers a number of advantages over single-molecule fluorophores and fluorescent proteins, such as improved signal/noise (S/N) ratio, higher photostability and facile chemistry of conjugation with targeting biomolecules due to numerous available reactive groups on the particle surface. Specifically, the overall fluorescence brightness from individual particles is proportional to the product of fluorescence efficiency and loading density of the encapsulated dyes; NPs usually fluoresce strongly when properly excited due to a large number of fluorophores resided in a single particle. Among a broad variety of photoswitches such as spiropyran (SP), spirooxazine (SO) diarylethene (DAE), azobenzene, stilbene, fulgide, rhodamine, and others, SP (SO) and DAE are two representative types of molecular photoswitches that were used as the light-responsive components for the construction of fluorescent photoswitches. [6, 23-25] In this review, we outline the major classes of SP/DAE-based photoswitchable fluorescent NPs developed in recent years while photoswitchable single-molecule fluorophores and fluorescent proteins, as well as NPs constructed from other types of photoswitches are beyond the scope of this review. Additionally, considering SP/DAE-based dynamic materials have been reviewed extensively, [6, 7, 26-29] we emphasize on the emerging applications of photoswitchable fluorescent NPs in biological fluorescence assays and detections with a few representative paradigms.

2. Structure of photoswitchable fluorescent NPs

Photoswitching fluorophores have found promising applications in detecting low-copy-number targets in high background noises and super-resolution imaging defying the diffraction limit. However, these photoswitches are expected to provide high contrast between the bright and the dark states for high detection sensitivity and super imaging resolution. Using single-molecule fluorophores as labeling reagents usually suffers from the problem of limited fluorescence brightness per labeled site. Additionally, single-molecule-labeled sites may suffer poor water-solubility, possible cytotoxicity, pH-dependent fluorescence emission, and rapid photobleaching, thus hindering the potential of successful applications. As an alternative strategy, integrating a large copy of fluorophores in a single nanoparticle has been proven as an effective way to increase the fluorescence brightness per probe (*vide supra*). It deserves mentioning that integrating dyes into NPs with optimized host matrix enables many advantages, including improved dispersity of probe in aqueous media and biocompatibility, reliable fluorescence signal output, facile incorporation of multiple tags for multiplex encoding, and the possibility of imparting the surface of NPs with diverse molecular functionalities. In this section, we review several types of photoswitchable fluorescent NPs with representative structural features, elucidate the underlying mechanisms, and evaluate the photoswitching performances.

2.1 Dye-incorporated photoswitchable fluorescent hybrid silica NPs

Among various host matrices for the construction of composite fluorescent NPs, silica is known to have overwhelming advantages of biocompatibility, versatility, mechanical integrity, excellent optical quality, and ease of chemical modification. More importantly, organic functional moieties can be easily incorporated into hybrid siloxane oxide networks. Thus, silica matrix was intensively used to host functional dye components for the construction hybrid organic–inorganic nanoprobes for various biological and medical applications. Using a sol-gel strategy, Bossi and co-workers fabricated silica-based photoswitchable fluorescent NPs by covalently incorporating photoactive component into the silica network.[30] Specifically, the photoactive

component consists of a rhodamine moiety linked to a photochromic DAE moiety with the former acting as the fluorescence-emitting moiety while the latter as the light-responsive one. As a representative photoswitch, DAE undergoes conversion from the open-form to the close-form upon UV illumination and can be switched back using visible light. The combination of light-driven interconversion between two states of DAE moiety with the Förster resonance energy transfer (FRET) mechanism between the rhodamine moiety and the DAE moiety is typically involved in the fluorescence photoswitching of these hybrid photoswitchable NPs.

Specifically, the close-form of DAE displays intense absorption band with maximum at 640 nm, which overlaps with the emission band of the rhodamine moiety. As a result, a FRET process between the rhodamine moiety (donor) and the close-form of DAE (acceptor and quencher) gives rise to fluorescence quenching of the donor and a fluorescent "Off" state was obtained. Upon illumination of visible light, the close-form of DAE can be switched to its open-form counterpart that does not display noticeable absorption in the visible region. Such conversion deactivates the FRET process between the rhodamine moiety and the DAE moiety and therefore restores the fluorescence emission. As a result, a fluorescent "On" state was obtained. Thus, reversibly activating and deactivating the FRET process between the rhodamine moiety and DAE components determines the fluorescent OFF/ON status of the NPs. More specifically, simply converting the photochromic components back and forth enables the fluorescence ON/OFF switching. Actually, the abovementioned mechanism is applicable to other FRET-based photoswitchable fluorescent systems, namely, modulating the fluorescence by activating and deactivating the FRET process between the fluorescence-emitting moiety and photochromic components at will.

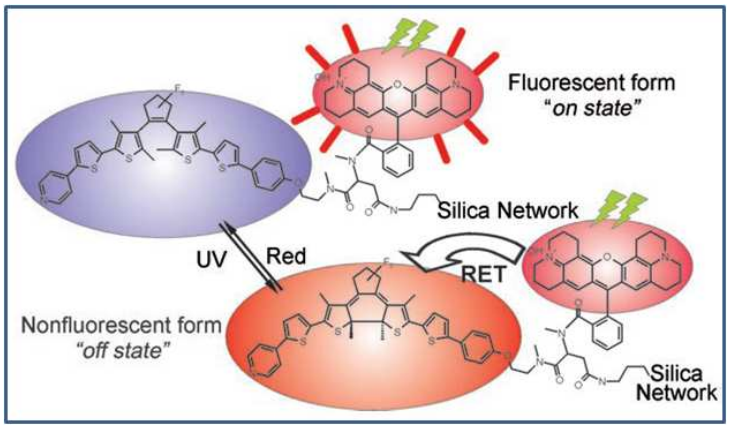

Figure 1. Chemical structure of the dyad photoactive unit contains photochromic DAE, fluorescent rhodamine and an inserted (3-aminopropyl) triethoxysilane moiety; the photochromic reaction underpins the fluorescence photomodulation. The photoactive units are covalently incorporated into the silica network via hydrolysis and condensation reactions. The generated photoswitchable NPs emit red light upon excitation of green light in the "On" state while FRET-enabled quenching prevents this emission in the "Off" state. Reprinted with permission from ref 30. Copyright (2008) John Wiley and Sons.

A noteworthy feature of the abovementioned silica-based photoswitchable fluorescent NPs is the photoactive dyad: the fluorescent emitter and photochromic quencher are at precisely 1:1 ratio. Such a strategy usually involves relatively complicated synthetic routes. Alternatively the fluorescent emitter and photochromic quencher can be integrated into the target NPs individually, which not only simplifies the synthetic procedure but also enables the tunable ratio of the FRET donor to acceptor in the final NPs for optimized efficiency of fluorescence quenching and higher On/Off contrast. Kim and co-workers fabricated photoswitchable fluorescent silica NPs via one-pot multicomponent copolymerization by mixing individual Cy3 (fluorescent emitter) and DAE (photochromic quencher) as reactive silane precursors simultaneously in the process.[31] Similar preparation strategies were also used to fabricate other silica NPs with photoswitchable fluorescence (or luminescence), including spiropyran and rhodamine,[32] DAE and rhodamine[33], DAE and fullerene [34], DAE and perylene diimide (PDI) pairs [35], respectively.

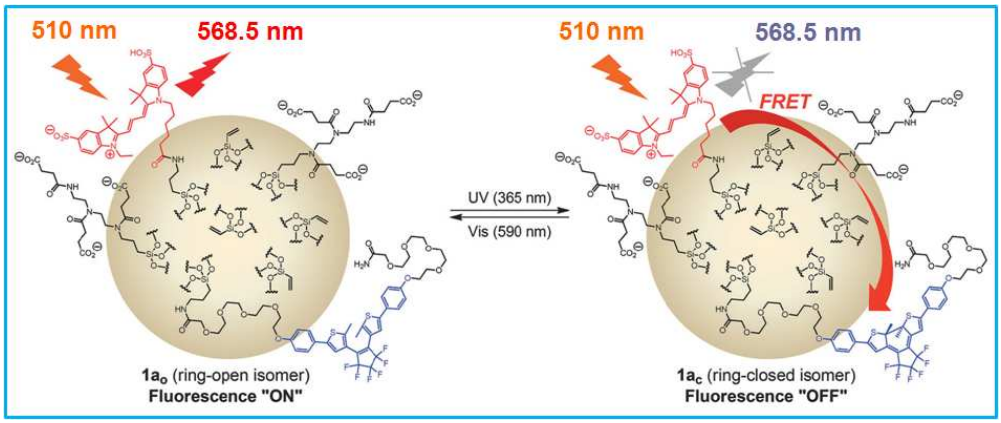

Figure 2. Photochromic DAE and fluorescent Cy3 dye are covalently incorporated into the silica network individually via hydrolysis and condensation reactions. The light-triggered reversible interconversion of DAE between its ring-open and ring-closed form activates and deactivates the FRET process between the DAE quenchers and Cy3 emitters, thus imparting fluorescence On-Off photomodulation. Reproduced with permission from ref 31. Copyright 2013 The Royal Society of Chemistry.

2.2 Polymer-based photoswitchable fluorescent NPs

2.2.1 Polymers matrix as container for carrying photoactive components

In analogy to silica, a polymer matrix also can be used as a container for carrying the photoactive components in the construction of photoswitchable fluorescent NPs. Specifically, the photoactive components can be either covalently incorporated into the polymer skeleton or physically embedded in the cross-linked polymer matrix. Using the strategy of radical-initiated microemulsion copolymerization, Li and coworkers fabricated hydrophobic-hydrophilic core-shell photoswitchable fluorescent polymeric NPs by covalently incorporating photochromic SP moieties into the hydrophobic polymer skeleton.[36] Specifically, the hydrophilic outer layer imparts dispersibility in aqueous media while SP moieties reside in the cross-linked polystyrene hydrophobic core, which separates the SP moieties from water and thus greatly enhances the photochemical (photoswitching) and photophysical properties (quantum yield).

As a typical photochromic component, SP can be reversibly switched between two isomers: the closed form SP and the open form merocyanine (MC). Neither SP nor MC fluoresces appreciably in water, although the MC form weakly fluoresces in

polar organic solvents and within self-assembled films. In sharp contrast, MC residing in the hydrophobic core of polymeric NPs is highly fluorescent and emits strong red fluorescence with emission maximum at 665 nm in aqueous solutions. Thus, the reversible SP-MC interconversion upon alternating UV and visible light illumination switches the red fluorescence of these polymeric NPs "On" and "Off"; the SP form is fluorescent OFF state while the MC corresponds to the ON state. In such systems, SP component is the only photoactive unit and acts as both the photochrome and the fluorophore simultaneously, virtually avoiding the involvement of additional fluorophore and circumventing the stringent requirements for FRET such as energy match, near unity energy transfer, and close proximity between the donor and the acceptor. Introducing additional fluorophores or modifying the molecular structure of SP compounds resulted in new types of polymeric NPs with dual-alternating-color photoswitchable fluorescence, either "blue-red" or "green-red".[37-39] Following similar strategies, photoswitchable fluorescent NPs were also constructed in other groups.[40-47]

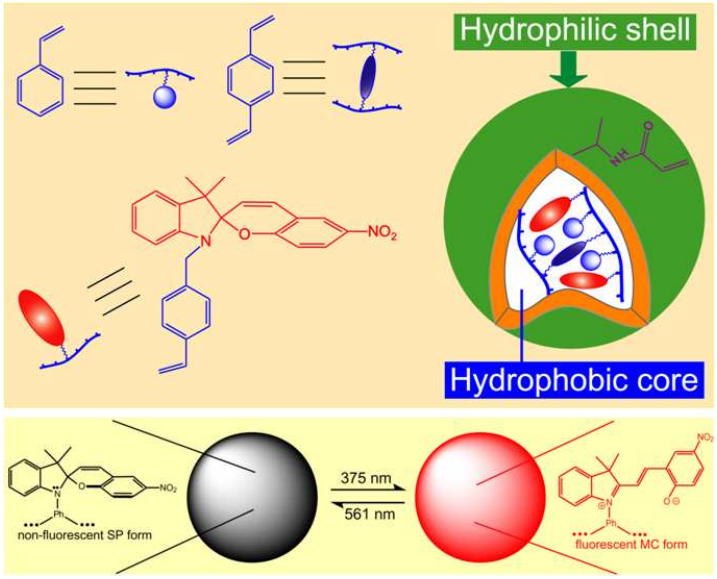

Figure 3. Photochromic SPs is functionalized with a styrene moiety and copolymerized with other monomers into the hydrophobic cavities of core-shell polymeric NPs via radical-initiated microemulsion copolymerization. Reproduced with permission from ref 39. Copyright 2013 John Wiley and Sons.

Entrapping BODIPY fluorescent dyes and photochromic SP components

noncovalently in the hydrophobic core of polymer micelles, Raymo and coworkers developed supramolecular nanoconstructs that possess photoswitchable fluorescence using an amphiphilic copolymer with hydrophobic decyl chains and hydrophilic PEG tails along a common poly (methacrylate) skeleton.[48] Based on a DAE amphiphilic molecular switch with hydrophilic tetraethylene glycol on one side and a hydrophobic chain on the other, another representative type of vesicle-like nanostructure with photoswitchable On/Off fluorescence was developed by Yi and coworkers. [49] Using a new type of SP-terminated poly (ε-caprolactone), Zhu et al recently re-precipitated biodegradable polymeric nanoparticles with photoswitchable fluorescence emission features. [50] In such a system, SP components were embedded in the hydrophobic poly (ε-caprolactone) matrix and their photochemical and photophysical properties were therefore similarly preserved as discussed above.

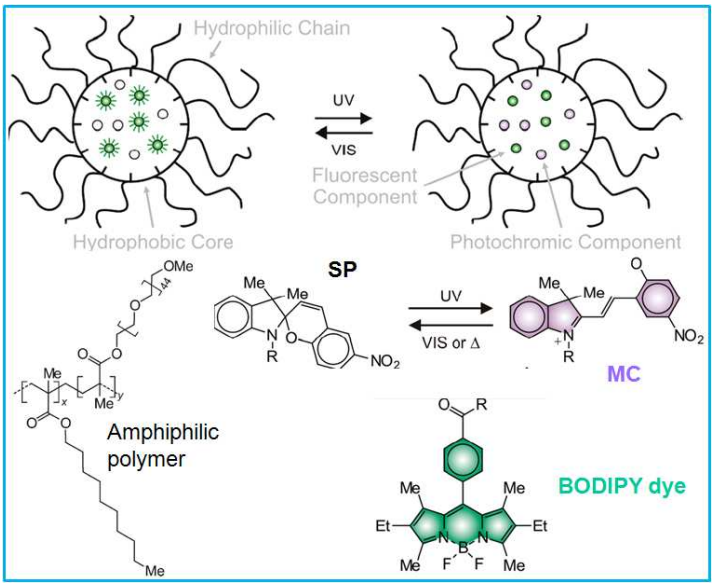

Figure 4. BODIPY derivative and spiropyran are embedded within the hydrophobic core of the supramolecular assemblies with an average diameter of 17 nm. Reprinted with permission from ref 48. Copyright (2011) American Chemical Society.

2.2.2 Conjugated-polymers based photoswitchable fluorescent NPs

In aforementioned polymer-based photoswitchable fluorescent NPs, the polymer matrix such as polystyrene (PS) and poly (methyl methacrylate) (PMMA) are optically inactive and they merely function as the container carrying the photoactive components. Conjugated polymers (CPs) are another class of macromolecules

characterized with delocalized π-conjugated backbones, which bestows them with high extinction coefficient and fluorescence emission features. Having high signal readout ability, good photostability and biocompatibility, particles made of CPs have emerged as a novel type of fluorescent probe with a variety of potentially useful optical properties for optoelectronic and biological applications. [51-54]

As pointed above, a common strategy for fluorescence photoswitching is to selectively quench the fluorophore's fluorescence via either electron transfer (ET) or FRET processes using the photochrome as a photoswitchable quencher. Thus, fluorescence photoswitching with maximal fluorescence contrast between the activated and quenched states relies on the fluorescence quenching efficiency. CPs possess unique advantages as the photoswitchable fluorescence donor because exciton diffusion in CPs generates amplified energy transfer or a super-quenching feature in the NPs by effectively funneling the excitation energy of multiple chromophoric units into a single quencher. [52]

Unequivocally, this type of amplified quenching is ideal for the fluorescence photoswitching with optimized fluorescence On-Off contrast. Applying such a design rationale, Harbron and coworkers developed a series of CPs-based fluorescent NPs with photoswitchable fluorescence features with various CPs as the fluorophore components while SO and DAE as the photochromes.[55-57] The combined amplified quenching and CPs resistance to photobleaching have improved photoswitching bright-to-dark ratio, photostability, and reversibility. Using a photochromic DAE derivative that can be switched between the colorless ring-open form and the ring-closed form with broad absorption up to the near-infrared (NIR) region as the optically controllable quencher and CPs capable of emitting the green and NIR fluorescence, Kim and coworkers developed CPs-based composite NPs with photoswitchable NIR fluorescence and demonstrated their ability for identifying imaging signals in thick biological samples. [58]

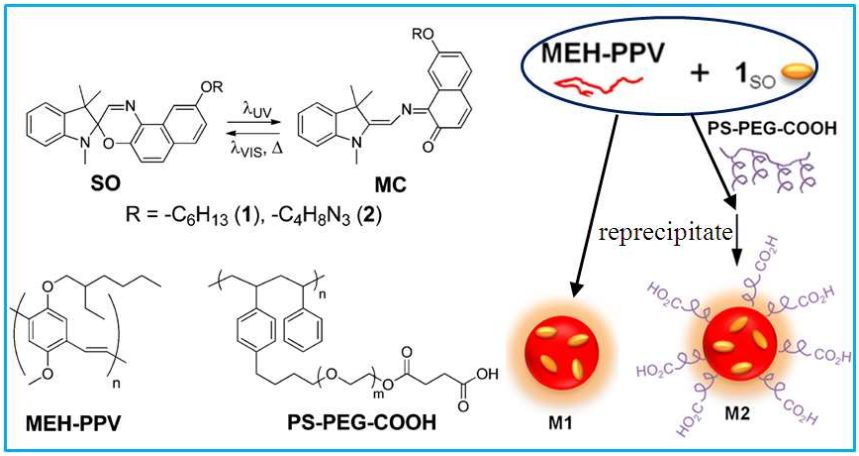

Figure 5. Photochromic spirooxazine (SO), fluorescent conjugated polymer MEH-PPV, and the amphiphilic polymer PS-PEG-COOH are entrapped to form NPs with possible functional carboxyl groups at the surface. Reprinted with permission from ref 57. Copyright (2014) American Chemical Society.

2.2.3 Dendrimer-based photoswitchable fluorescent NPs

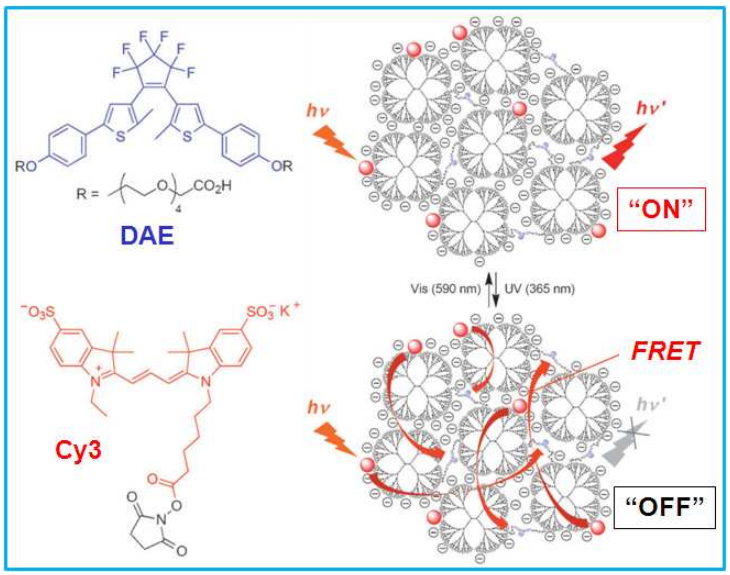

Figure 6. Amine-terminated dendrimers oligomerized into nanoclusters that were crosslinked by a DAE derivative bearing reactive carboxylic moieties on both ends. Furthermore, fluorescent Cy3 dyes were attached to the amines via activated esters. Reprinted with permission from ref 59. Copyright (2012) John Wiley and Sons.

Fluorophores with highly extended π-conjugation are prone to aggregate when they are positioned in close proximity to each other. With the purpose of constructing probes with maximal fluorescence On-Off contrast and minimal aggregation-induced fluorescence-quenching, Kim and coworkers developed dendrimer-based photoswitchable fluorescent NPs by sparsely attaching fluorescent dye moieties at the

fifth generation polyamidoamine dendrimer and using photochromic DAE derivative with reactive carboxylic moieties on both end to cross-link oligomerized dendrimers. [59] This strategy of minimizing fluorescence self-quenching has produced on–off contrast of 6.0-19.1 in living systems.

2.3 Photoswitchable and photoluminescent hybrid NPs

Among the broad spectrum of fluorescent/photoluminescent NPs used as imaging probes, quantum dots (QDs) undoubtedly occupy a special niche due to their unique photophysical features such as high luminescence quantum yield, desired photostability, broad excitation and narrow emission spectra, and distinctive emission lifetimes. These advantages impart QDs as attractive candidates for a diversity of biological imaging and sensing applications. [60] Another important inorganic luminescent material is the upconversion nanophosphors (UCNPs) capable of converting two or more low-energy near-infrared (NIR) photons into a higher-energy visible photon. [61, 62] However, these inorganic nanoparticles are not photoswitchable by themselves. After these inorganic nanoparticles are properly conjugated to organic photochromic molecules, the resulting surface-modified hybrid particles gained reversible interconversion between bright and dark states via either photoinduced electron transfer (PET) or FRET mechanism.[26, 63] Indeed, many QDs and UCNPs with photoswitchable luminescence emission features were fabricated using this strategy.[64-74]

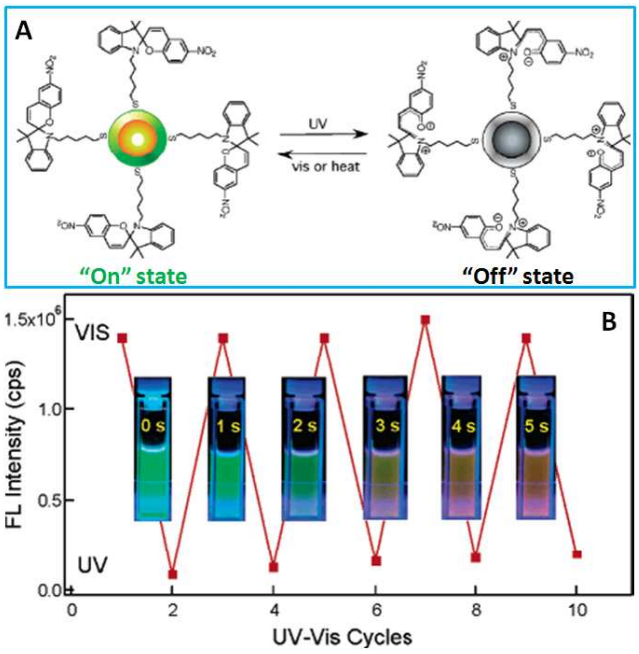

Figure 7. A) Core-shell CdSe/ZnS QDs with surface-functionalized spiropyran moieties exemplify reversible luminescence On/Off photoswitching. B) Visible and UV light reversibly switches luminescence of the NPs on and off. The overlay demonstrates luminescence switching in ~5 s under UV illumination (365 nm). Reprinted with permission from ref 65. Copyright (2005) American Chemical Society.

Li and co-workers imparted photoswitchable luminescence in QDs by anchoring SP components on the surfaces of core-shell CdSe/ZnS QDs via a thiol-metal linkage. [65] As a representative class of photoswitch, SP molecules typically undergo reversible interconversion between a ring-closed state (spiropyran, SP) and a ring-open state (merocyanine, MC) upon alternating UV/Vis illumination. Specifically, MC species display intense absorption in the visible region, which has a good overlap with the emission band of CdSe/ZnS QDs, enabling FRET from QDs to MC moieties. In such case the luminescence of QDs is quenched and the hybrid NPs act as the "Off" state. Upon illumination with visible light, MC are switched back to their counterpart SP species that do not absorbs in the visible region and therefore the FRET process that lead to luminescence quenching of QDs are deactivated due to energy mismatch. In such a way, the photo-induced reversible interconversion of SP between two states with distinct absorption features effectively controls subsequent FRET and modulates the luminescence emission of QDs, thus eventually enabling photoswitchable

ON/OFF luminescence emission of the hybrid NPs. Actually, such a general fluorescence/luminescence photoswitching mechanism was successfully confirmed in many other similar systems.

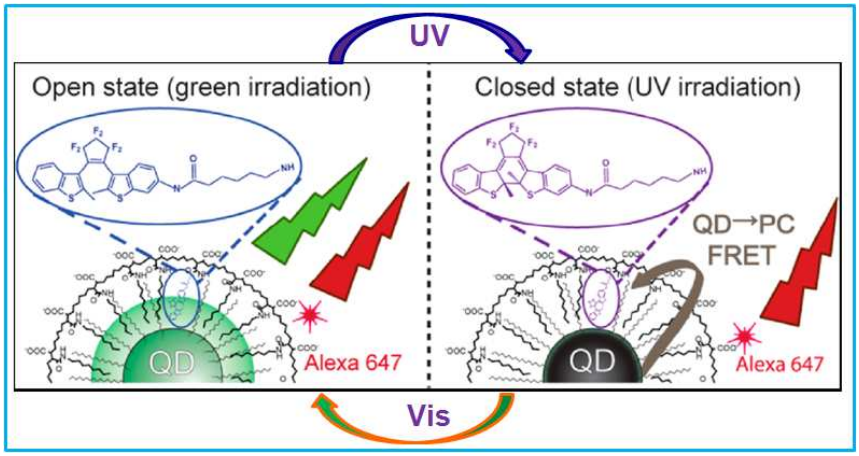

Figure 8. The surfaces of QDs are coated by amphiphilic comb polymer with pendant photochromic DAE moieties. Fluorescent Alexa647 dye was adsorbed via hydrophobic interactions between the aliphatic chains with the lipophilic ligands on the QDs surface. The luminescence of the QD is modulated by the photoconversion of the DAE component while the Alexa647 acts as the internal fluorescence standard. Reprinted with permission from ref 70. Copyright (2012) American Chemical Society.

Jovin and coworkers constructed a new type of photoswitchable QDs characterized with dual-color, ratiometric sensing and imaging capabilities. This type of NPs was fabricated by coating the luminescent QDs with an amphiphilic photochromic polymer and a second fluorescent dye. Specifically, the second dye Alexa 647 was employed as an internal standard and its red fluorescence (666 nm) intensity was used to gauge the green luminescence (550 nm) of the QDs being modulated on-and-off by the photochromic DAE via the controlled FRET. As a result, a tunable green-to-red emission ratio of the hybrid photoswitchable NPs upon alternative UV/Vis illumination was achieved. [70] Following this rationale, Jovin and coworkers further fabricated another type of dual-color photoswitchable NPs on the basis of modulating FRET between the fluorescent dye Lucifer Yellow (LY) and the photochromic DAE moiety using QDs as a template and an internal standard. [71]

Branda and coworkers developed UCNPs with photoswitchable luminescence features by attaching photochromic DAE components onto the surfaces of UCNPs via

a copper-catalyzed cycloaddition "click" reaction.[73] Specifically, upconversion of the UCNPs converts the near infrared 980-nm excitation into visible fluorescence, which overlaps well with the absorption band of the ring-closed isomer of DAE components, thus enabling FRET-based quenching of the UCNPs luminescence. Upon photoswitching the DAE photochrome to its ring-open form using visible light, the ring-opened DAE is unable to quench the upconverted luminescence, thus the UCNPs are in the bright state. Conversely when the DAE photochrome is photoswitched to its closed form, the upconverted luminescence is quenched and the UCNPS are in the dark state. Similar upconversion systems using dual-color photoluminescence was also developed in Yan's group by covalently grafting photoswitchable SP moiety on the surface of silica-coated UCNPs that typically exhibits a green emission band (~540 nm) and a red emission band (~660 nm) upon excitation at 980 nm. Specifically, the green emission band of UCNPs appreciably overlaps with the absorption band of the ring-closed SP form while the red emission band does not. Thus, optically switching the photochromic moiety between its ring-closed SP and ring-opened MC state either activates or deactivates the FRET process from the UCNP to the photochromic moieties. The net result is that green emission band of UCNPs can be photoswitched on-and-off while the red emission band nearly remains unperturbed. Such a unique system enables green luminescence on-and-off modulation and has a constant red emission serving as an internal standard without the complication of adding a second fluorescent dye.[74]

3 Emerging applications using photoswitchable fluorescent NPs

3.1 Photoswitchable fluorescent NPs enable high-resolution imaging

Fluorescence imaging has become an indispensable tool for visualizing dynamic protein interactions, intracellular networks, and material transport in living cells and revealing biological mechanisms in real time. However, the diffraction limit originating from the wave property of light restricts the optical microscope resolution to ~300 nm, a level two of orders of magnitude coarser than nanoscaled molecules; thus many intracellular organelles and their associated molecular structures remained

unresolvable. Several ultrahigh-resolution fluorescence microscopic techniques developed in recent years have circumvented the diffraction limit, capable of achieving images with 20-30 nm lateral and 50-60 nm axial resolutions in biological fluorescence imaging. The controllable fluorescence on-off photoswitching plays critical role in these revolutionary ultrahigh-resolution imaging techniques. [7, 27, 29, 75-79]

The bottleneck is that multiple emitting fluorophores located within the diffraction-limited area cannot be resolved simultaneously. However, if only one fluorophore is emitting at a given time, then its location can be determined down to nanometer accuracy, far beyond the Abbe diffraction limit. Using this principle, super-resolution imaging techniques capable of revealing previously unimagined subwavelength details, including photoactivation localization microscopy (PALM or FPALM),[19, 20] stochastic optical reconstruction microscopy (STORM), [18] photoactuated unimolecular logical switching attained reconstruction (PULSAR) nanoscopy, [22] and others, [21] have been developed.

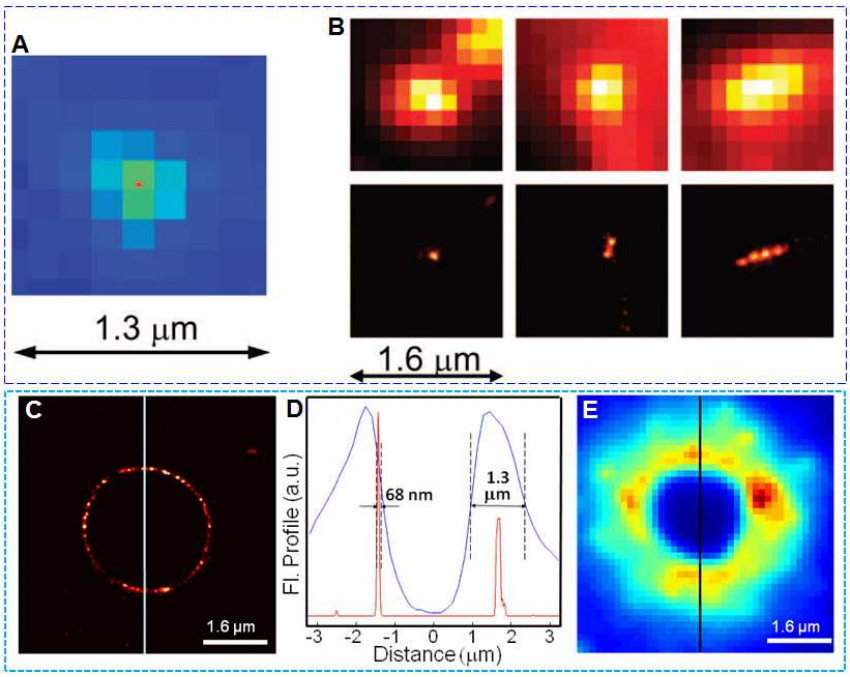

Figure 9. (A) The position of a single molecule is precisely located by determining its centroid position at nanometer precision. (B) PULSAR nanoscopy easily resolves one, two, or four NPs within a diffraction-limited area, whereas conventional microscope cannot. (C) PULSAR image exemplifies typical circular structure of a nanoparticle monolayer surrounding an amorphous $CaCl_2$ microstructure. A vertical line is drawn

in the same position of the high-resolution image (C) and diffraction-limited image (E). (D) The fluorescence profiles from PULSAR and conventional techniques are plotted for the vertical line. Reprinted with permissions from ref 22 and 80. Copyright (2008) American Chemical Society and (2011) The Royal Society of Chemistry.

Using SP-based photoswitchable polymeric NPs, [38] Li and coworkers developed PULSAR nanoscopy technique and achieved biological fluorescence imaging with resolution down to 10-40 nm. [22, 80] For the SP-containing polymeric NPs, the SP form has negligible visible absorption and consequently no fluorescence under visible excitation while its counterpart ring-opened form MC absorbs intensely at 570 nm and emits vivid red fluorescence (665 nm) in hydrophobic NPs cores. Alternating UV/vis illumination induces reversible SP-to-MC conversion and therefore switches fluorescence on-and-off. Instead of photobleaching, PULSAR strategy generally images photoswitchable NPs first and then switches it off. Because SP has no absorption at MC band region, it cannot be photobleached by exciting into the MC absorption band. For biological fluorescence imaging, such performance is unequivocally significant because all interfering fluorophores that emit under the imaging laser can be photobleached before imaging begins, which provides an effective method to reduce interfering fluorescence for single-molecule experiments.

In a typical PULSAR imaging cycle, a short 375-nm UV pulse was used to convert a few sparsely resided SP molecules into the emitting MC bright state and subsequently a regular 532-nm excitation pulse were employed to acquire the single-molecule fluorescence image of the MC component. Simultaneously, imaging laser converted the emitting MC into non-emitting SP. The location of a single SP/MC molecule can be determined with nanometer precision by fitting its experimental single-molecule image to a Gaussian mask (Figure 9A). By repeating such imaging cycle, multiple frames embodying large number of locations of single-molecule emitters can be obtained. Summing many accumulative individual frames with precise location of each single-molecule reconstructed the final super-resolution image. As compared to the traditional fluorescence imaging technique, PULSAR microscopy provides a dramatic resolution improvement. While traditional fluorescence microscopy cannot resolve four SP-containing photoswitchable NPs arranged in a row,

PULSAR microscopy clearly resolves the nanostructure composed of four juxtaposed NPs on glass (Figure 9B). Figure C and E compare the PULSAR image to the traditional microscopic image of a nanoscaled pattern formed via self-organization of SP-containing photoswitchable NPs around an amorphous $CaCl_2$ circular structure. The PULSAR image yields a FWHM of 68 nm, whereas the conventional microscopy produces a FWHM of 1.3 μm (Figure 9D).

3.2 Photoswitching enables super-brightness in frequency-domain imaging (FDI)

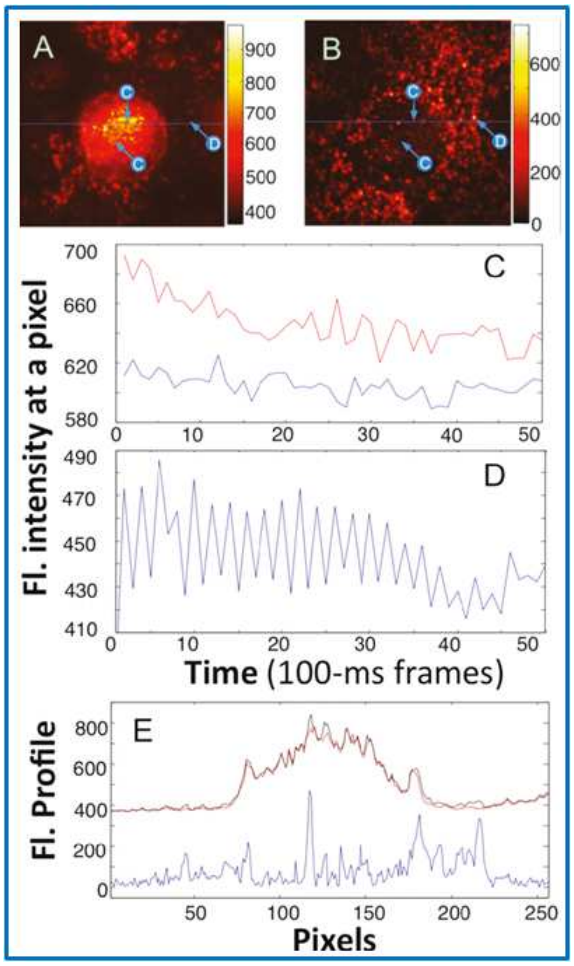

Figure 10. (A) The time-domain image of polystyrene-based circular pattern with embedded Nile Red dye (spots labeled with C) and SP-containing polymeric NPs (spot labeled with D). (B) PFT images of the same area illustrated in (A) essentially removed the spots labeled with C and greatly amplified the spots labeled with D. (C, D) The fluorescence profiles of labeled spots reveal the insight of the above phenomena. The spots labeled with C are non-periodic, either linearly or exponentially decay in time; whereas the spots labeled with D are periodic with the unique photoswitching frequency. (E) Comparing time-domain with frequency-domain fluorescence intensity

traces along the lines in (A) and (B) reveals that although interference dominates the time-domain data (red and black traces), single-molecule emitters can be detected in the presence of overwhelming interference (blue) in frequency domain. Reprinted with permission from ref 81. Copyright (2011) American Chemical Society.

The probe brightness is undoubtedly of great importance in biological fluorescence imaging in terms of elucidating the signals of interest from complicated physiological environments with high levels of background. However, a single probe usually has limited brightness in time domain imaging that usually renders individual molecules undetectable in the presence of interference, such as interfering fluorescence or cell autofluorescence. Thus, boosting probe brightness represents a daunting challenge in single-molecule detection in biological and biomedical research. Taking the advantage of fluorescence photoswitching features of the SP-containing polymeric NPs, Li and coworkers developed photoswitching-enabled Fourier transform (PFT) fluorescence microscopy capable of continuously amplifying the brightness of the modulated probe while suppressing the non-modulated interference signals.[81] The underlying mechanism of such powerful PFT imaging technique involves the selective response in fluorescence emission of the photoswitchable NPs to the external periodic optical stimuli. Specifically, the simulation results reveal that periodically oscillating fluorescence signals could be amplified in the frequency domain via photoswitching-enabled Fourier transform (PFT) while other types of signals, including those that evolve linearly, exponentially, constantly, and on-and-off like blinking are significantly suppressed upon signal modulation-and-demodulation. Thus, the photoswitchable fluorescent NPs can be made super bright in the frequency domain simply by acquiring more fluorescence on-and-off modulation cycles in the time domain and the undesired interfering fluorescence or noise can be mostly removed from the signal of interest even if the interfering fluorescence or noise have the same color as the probe or are orders of magnitude stronger than the modulated signal.

In time-domain imaging (Fig.10A), the circular polystyrene areas with embedded fluorescent Nile Red dye emit the strongest fluorescence in the image, seriously

obscuring the SP-containing NPs on or near it. In sharp contrast, frequency-domain imaging dramatically reveals SP-containing single-particle (Fig. 10B) while the non-modulated interfering fluorescence signals of Nile Red dyes are remarkably suppressed. Fig. 10C illustrates two typical interfering fluorophore trajectories: one decays exponentially (the red curve) while another decays linearly (the blue curve). In the PFT imaging, both of these two signals oscillate randomly and contribute very little to the PFT intensity at the locked frequency. Thus, the corresponding interfering spots labeled C in (A) and (B) are dark in the frequency domain (Fig 10B), although they emerge as the brightest spots in the time domain (Fig 10A). Fig 10D displays the evolution of a signal oscillating at a locked frequency (2.32 Hz) (labeled D in Fig 10A and Fig 10B). This signal is nearly completely obscured by the strong Nile Red interference in the time domain but dramatically burst into a very bright spot in frequency-domain imaging. Fig. 10E shows the fluorescence intensity profiles along the thin blue line in both Fig. 10A and Fig. 10B. The red and black curves in the upper panel are fluorescence intensity acquired before and after photoswitching. It can be seen that intensity from the probes becomes more obvious and even NPs on top of the polystyrene circular pattern become visible at this lower interfering scale. In sharp contrast to the difficulty in resolving single-particle emitters using time-domain data, revealing individual particles with satisfactory resolution via the frequency-domain strategy is achieved with ease after signal amplification and interference suppression (the blue curve in Fig. 10E).

3.3 Antiphase dual-color correlation imparts ultrasensitivity

Rarely, a single molecule can function as a photochrome, a green emitter, and a red emitter, but such a molecule was discovered in a modified spiropyran–methoxy spiropyran (MSP). Using photoswitchable NPs containing MSP–a dual-alternating-color emitter, [38, 39] Li and co-workers recently developed an antiphase dual-color (AD) correlation imaging strategy capable of greatly improving the S/N ratio and therefore enhancing the ultimate detection limit in fluorescence imaging.[82] Reversible interconversion between methoxyspiropyran (MSP)-methoxymerocyanine

(MMC) in polymeric NPs correspondingly switches fluorescence between green color (λ_{max} = 530 nm) and red color (λ_{max} = 665 nm). Because MSP and MMC are linked via two reversible photochemical reactions, their fluorescence properties are also correlated in the same manner. Thus, alternating UV or NIR and visible illumination generates the reversible cycle between the green and red fluorescence. Importantly, such clean one-to-one conversion intrinsically enables a time delay between the green and red fluorescence and therefore green-to-red fluorescence toggling in an antiphase manner, rather than a simple fluorescence on-off modulation. Consequently, red fluorescence of the NPs reaches maximum at even phase (2π, 4π, 6π, etc.) while the green fluorescence is maximized at odd phase (π, 3π, 5π, etc.).

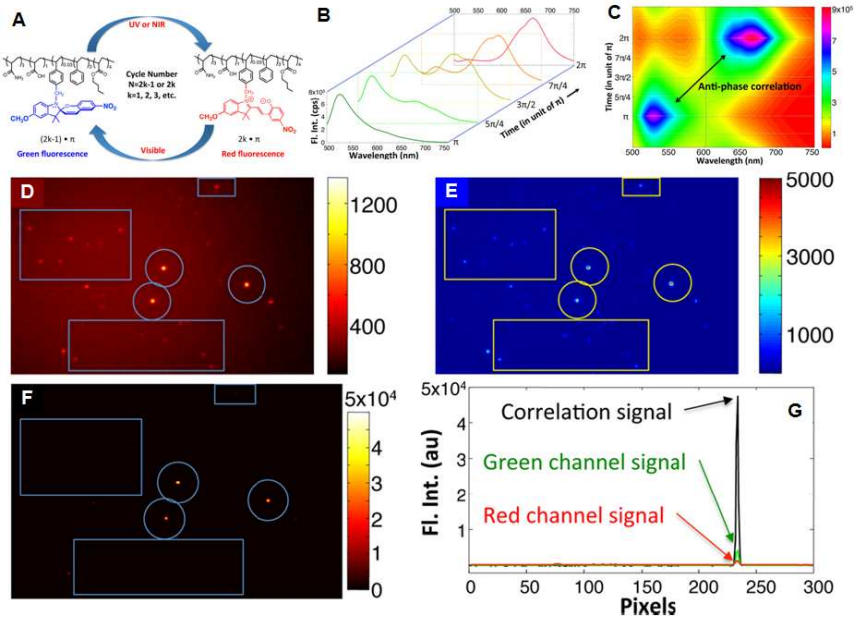

Figure 11. (A) UV or NIR light drives the conversion of green-emitting polymeric NPs containing MSP into the red-emitting NPs containing MMC, and visible light drives the reverse process. (B) Spectral evolution showing the photochemical conversion of green-fluorescing NPs to red-emitting NPs over the time period of π. (C) Two-dimensional contour plot revealing the AD correlation or half-period of π shift between the green and red maxima. (D, E) Green and red images acquired based on the integrated fluorescence intensities. (F) AD correlation imaging removes those signals that have no such correlation (signals in boxes) and enhance those from AD NPs (signals in circles). (G) Line profiles passing through AD NPs reveal that the intensities of the correlation signals are orders of magnitude larger than those of the single-channel integrated signals (D or E). Reprinted with permission from ref 82. Copyright (2015) American Chemical Society.

Based on such intrinsic antiphase correlation between the red and green

fluorescence from a single molecule, AD correlation imaging microscopy was developed by defining the signal intensity of each cycle as the product of the dual-color fluorescence minima subtracted from the product of the dual-color fluorescence maxima as given in the following:

$$P_{\mathrm{corr}}(i, j) = \sum_{k=1}^{N/2} [P_{\mathrm{green}}(i, j, (2k-1)\pi) P_{\mathrm{red}}(i, j, 2k\pi) - P_{\mathrm{green}}(i, j, 2k\pi) P_{\mathrm{red}}(i, j, (2k-1)\pi)]$$

where $P_{\mathrm{corr}}(i, j)$ represents the signal intensity at position (i, j) in the AD correlated image. The same pixel displays the green fluorescence with maximum intensity $P_{\mathrm{green}}(i, j, (2k\text{-}1)\pi)$ and its concomitant red fluorescence minimum $P_{\mathrm{red}}(i, j, (2k\text{-}1)\pi)$ at odd π, whereas the green fluorescence minimum $P_{\mathrm{green}}(i, j, 2k\pi)$ and its concomitant red fluorescence maximum $P_{\mathrm{red}}(i, j, 2k\pi)$ occur at even π.

Fig. 11D, E displays the fluorescence images acquired via the green (505-543 nm) and red (610-800 nm) channels, respectively, with the antiphase signals in circles and non-antiphase signals in boxes. Processing every individual pixel (i, j) using the above equation produces the AD correlated image in Figure 2F, in which all of the interfering signals and noise in the boxes disappeared while the alternating dual-color signals significantly augmented with the intensity scale jumping by an order of magnitude. In AD correlation image, the interfering signals and noise were removed by the second term in the equation due to their non-photoswitching nature while signals from the dual-color molecules were amplified. Such AD-correlation-enabled suppression of noise and the concomitant amplification of target signal impart significantly improved S/N ratios in the final fluorescence images (Fig. 11G). Specifically, the S/N ratios in the green and red channels at a circled spot are 132 and 43.3, respectively. In sharp contrast, the S/N ratio in the AD correlation is improved up to 825, with amplification factors of 6.25 and 19 as compared to those of the green and red channels, respectively.

3.4 Dual-alternating-color correlation fluorescence imaging

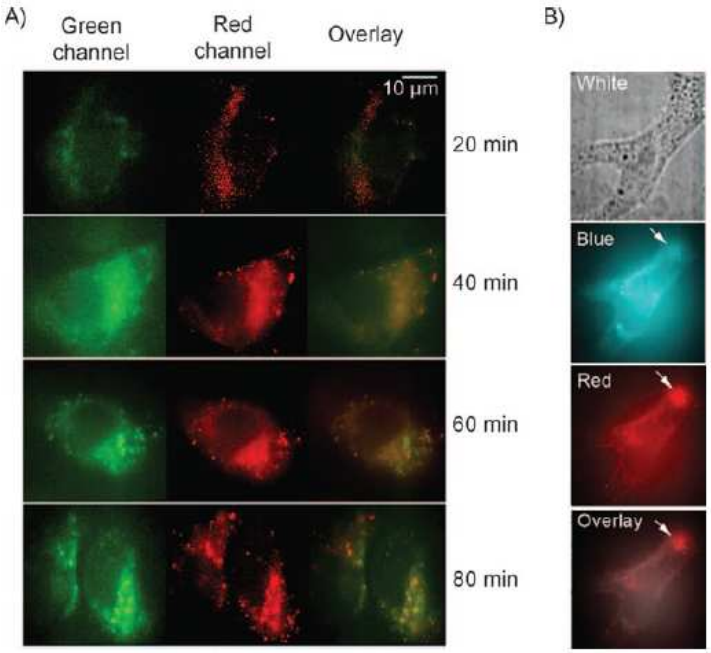

Figure 12. (A) Polymeric NPs with green-to-red dual-alternating-color fluorescence features undergo endocytosis as time elapses. Cells collect these endocytosed cargoes into lysosomes and hence multiple confined NPs manifest as brighter spots. (B) The most intensive red-fluorescence spot (arrow) is unveiled to be a false positive because its signal cannot be corroborated in the blue channel. Reprinted with permission from ref 38. Copyright (2009) American Chemical Society.

Fluorescent NPs that can be optically switched between two fluorescence colors, for instance green and red colors, are capable of highlighting themselves by producing signals of different colors with encoded intrinsic correlations. Owing to their unique ability for highlighting the same spot of interest with two distinct colors, employment of these dual-alternating-color photoswitchable fluorescent NPs can effectively circumvent the cellular fluorescence interfering problems such as autofluorescence. Such an intrinsic relationship between fluorescence signals acquired via two channels virtually enables unambiguous detection of the target probes from the interfering fluorescence and noises, a statistical confidence that other types of probes do not have. Figure 12 displays living-cell fluorescence imaging using dual-alternating-color photoswitchable fluorescent NPs, in which photoswitching converts the fluorescent NPs from emitting green or blue to red reversibly. For instance, MSP-containing NPs alternately emit red (λ_{max} = 665 nm) and green fluorescence (λ_{max} = 530 nm) with an

antiphase correlation. Such two independent fluorescence-imaging channels unambiguously verified the locations of target NPs in cells (Fig 12A). In summary, only those spots that emit in both channels truly originate from the NPs while other areas with a single color might represent false positive signals from either interfering emitters, even if they fluoresce the same color as one of the alternating color that the photoswitchable NPs emit. Fig 12B presents such an example, where dual-color photoswitchable NPs having blue-to-red fluorescence switching features were used as probes for living cell imaging. The intensive red-fluorescence region indicated by an arrow has no blue counterpart, and therefore it was assigned as a false positive even though its intensity dominates the image.[38]

3.5 Photoswitching-based phase-sensitive lock-in fluorescence detection

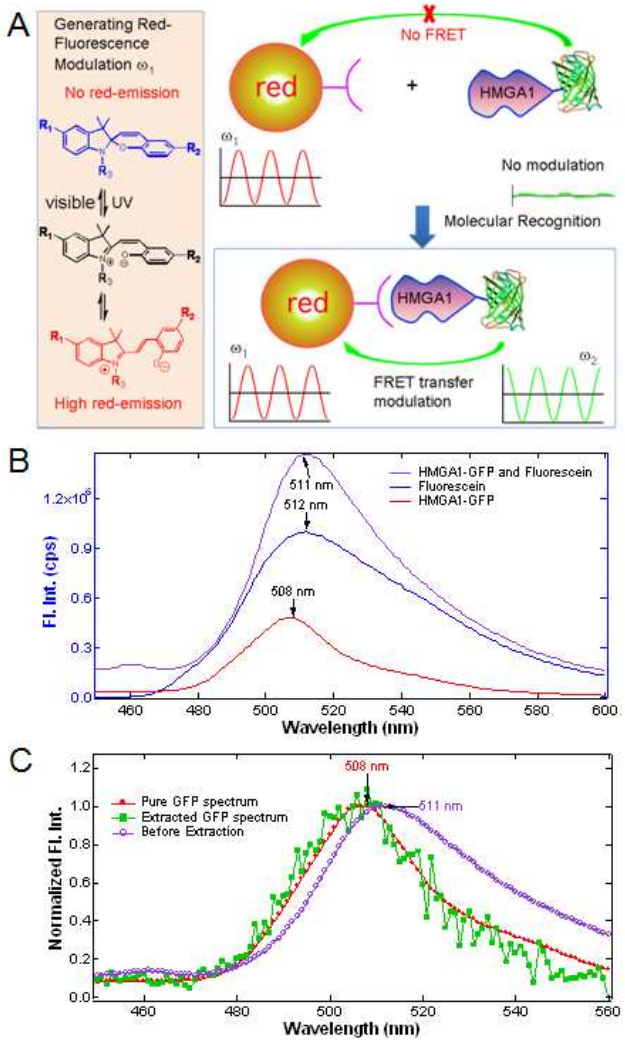

Figure 13. (A) Schematic representation illustrating photoswitching-induced fluorescence modulation of SP-containing NPs (red-fluorescence modulation) and the lock-in fluorescence-modulation-transfer from NPs to green fluorescent proteins (green-fluorescence modulation) based on modulating FRET efficiency. (B) Fluorescence spectra of HMGA1-GFP (red), fluorescein (blue), and their mixture (purple) at a 1:2 fluorescence ratio. (C) Because the maximum of fluorescein noise emits at nearly identical region (512 nm) and is twice stronger than the intensity of GFP signal at 508 nm, it completely obscures the GFP signal. Photoswitching-induced double modulations cause the GFP signal to oscillate, but not the fluorescein noise, thus, successfully separating the GFP emission spectrum (green squares) form the large noises (purple open circles). Reprinted with permission from ref 89. Copyright (2011) American Chemical Society.

In fluorescence-based bioanalysis, precisely identifying biological targets and accurately extracting their relatively weak signals from complicated physiological environments represent daunting challenges. Increasing efforts have been devoted to solution for distinguishing the fluorescence signals of interest in complex samples that often produce background noise, autofluorescence and interferences. Dickson and co-workers demonstrated that via the approach of dual-laser coillumination, in which the secondary laser with longer wavelength than that of the laser for fluorescence acquisition is responsible for optical depopulation of the photoinduced long-lived dark state of the fluorophore and the regeneration of the emissive state, selective fluorescence enhancement and highlight of weak signals of target from large backgrounds can be achieved.[83] Based on such strategy of dark state engineering and secondary laser illumination, examples of selective recovery of the signal of interest by removing heterogeneous background emitter signals and direct extraction of desired fluorescence from high background were also demonstrated in the same research group. [84-88]

Using the frequency feature of the photoswitchable NPs, Li and co-workers developed a fluorescence analysis strategy on the basis of optical lock-in detection (OLID) principle for separating the frequency-modulated signals of target from strong interferences.[89] In such strategy, the fluorescence modulation is based on the photochemical reaction and constant excitation source was employed, fundamentally

different from the abovementioned fluorescence modulation based on the modulation of the secondary excitation source. The net result is that the red fluorescence of the SP-based NPs and the green-fluorescence of GFP are modulated at will with a specific and unique locked frequency (Fig. 13 A).

Photoswitching of SP-containing photoswitchable NPs generates periodic red fluorescence undulation in sync with the in-phase oscillation of the absorption in the visible region with the latter in turn inducing fluorescent donors within the Förster proximity to undulate in a locked frequency. The FRET is a short distance phenomenon and typically plummets quickly after the Förster distance. Thus, only fluorescence of the labeled analytes that are recognized by the photoswitchable NPs can be modulated via the FRET process while fluorescence of the interfering fluorophores remains far away from the NPs, thus outside the Förster proximity. Therefore, fluorescence interferences will not oscillate with the locked-frequency even if the interfering fluorescence has much higher intensity with spectrum closely resembles that of target. In the case of detecting the fluorescence signal of GFP (analyte) in the presence of fluorescein (interference) with much stronger intensity, as shown in Figure 13, the crude OLID data contained the superposition of both frequency encoded HMGA1-GFP signal and the fluorescein noise. By applying a reference waveform conformed to photoswitching profile of photoswitchable NPs and using the modulation frequency as the intelligent information for data separation, the "real" spectrum of HMGA1-GFP can be extracted and revealed after several complete photoswitching cycles. The conclusion is that frequency-modulated signals can be easily separated from noise even if the latter are 10 times stronger that the former.

3.6 Reversible two-photon photoswitching and two-Photon Imaging

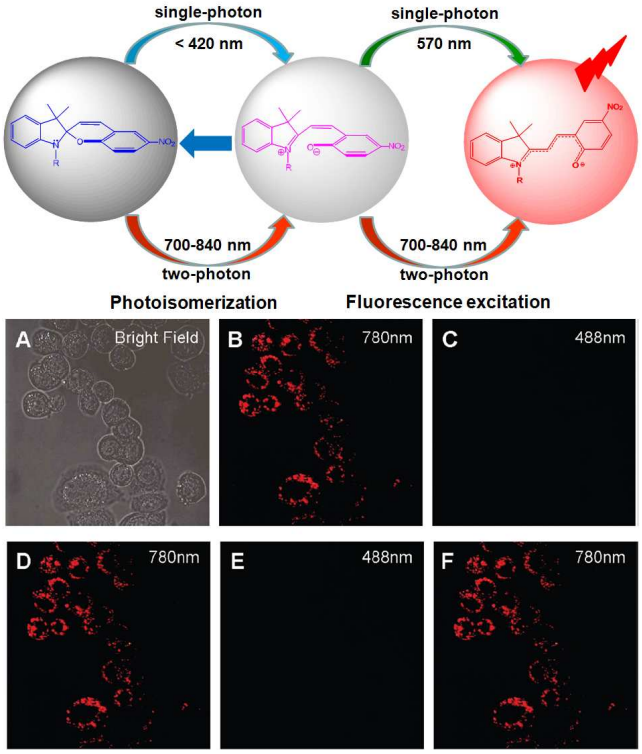

Figure 14. The SP-containing polymer NPs can be switched from "off" to "on" via illumination of either UV light (<420 nm) or NIR light (700-840 nm) via a two-photon absorption mechanism and then imaged using either visible light (<570 nm) or NIR light (700-840 nm) as the excitation source (Upper panel). Bright-field imaging of SK-BR-3 cells labeled with anti-Her2 antibody-conjugated photoswitchable nanoparticles (A). Two-photon photoswitching and two-photon imaging at 780 nm of Her2 receptors on the cellular membranes switch on red-fluorescence (B). Single-photon excitation at 488 nm switches off red fluorescence (C). This on-off photoswitching can be repeated ≥20 times (C-F). Reprinted with permission from ref 90. Copyright (2011) American Chemical Society.

Most of the photoswitchable fluorescent NPs developed to date, such as the aforementioned SP- and DAE-based photoswitchable probes, are generally activated via high-energy UV or near-UV light, which can induce undesired physiological changes in cells and therefore give rise to photodamage to biological samples. Additionally, the use of short-wavelength UV or near-UV light in biological applications generally suffer from the limited penetration depth of light in investigating deep-seated target and thick samples owing to the high levels of scattering. Strategies for mitigating the UV-induced photodamage and circumventing the impediment of penetration depth in photoswitching-based biological applications

are thus desirable; particularly those can be performed using NIR light as the activation and excitation source. Zhu and co-workers developed NPs that can be photoswitched and imaged by NIR 780-nm light.[90]

The SP molecules residing in the polymer NPs can be optically switched to its counterpart isomer MC upon 780-nm excitation via a two-photon absorption (TPA) mechanism, thus avoiding harmful UV light (Fig.14). Additionally, the 780-nm NIR light can also serve as the excitation for fluorescence-image. The NIR light cannot switch the MC molecules back to SP molecules, but visible light such as 488 nm can. These polymeric NPs was immunofunctionalized with anti-Her2 antibody, which specifically binds to Her2 receptors on the surface of SK-BR-3 cells after incubation, and the complete cycle containing sequential TPA-based switching on, TPA-based imaging, and visible light-induced switching off of the NPs in live cell was demonstrated (Fig. 14F).

3.7 Photo-rewritable fluorescence patterning for optical data storage

From the technical viewpoint of optical data storage, reversible fluorescence photoswitching, either on-and-off or dual-alternating-color conversion, intrinsically constitutes the basis for reversible data encoding (writing) and erasing, despite many practical issues standing in the way of working devices. Actually, fluorescent materials with photoswitchable emission features have been suggested as potential candidates for optical data storage media at both single-molecule and nanoscale level .[91-94] Figure 15 illustrates the proof-of-principle for rewritable data storage in 2D using the polymeric NPs with photoswitchable fluorescence as the medium. Typically, the spotted pattern prepared by placing photoswitchable polymer NPs within selected wells of a 96-well microplate displayed vividly red fluorescent photopattern upon short time UV-irradiation (Fig. 15A). The following 30-min illumination of visible light made the pattern completely disappear. Subsequently, the photoerased pattern can be restored upon exposure to UV-irradiation. This red fluorescence on-and-off cycle can be repeated many times, and dried films with embedded photoswitchable polymeric NPs display similar fluorescence on-off phenomena.[36] Using BODIPY as

fluorophore and photochromic SP as the photoswitching modulator, Chen and coworkers recently developed photoswitchable fluorescent polymeric NPs with dual-alternating-color fluorescence and demonstrated the potential of photoswitchable fluorescent NPs in fabrication of photorewritable fluorescence patterning for data storage, as shown in Figure 15 B.[95]

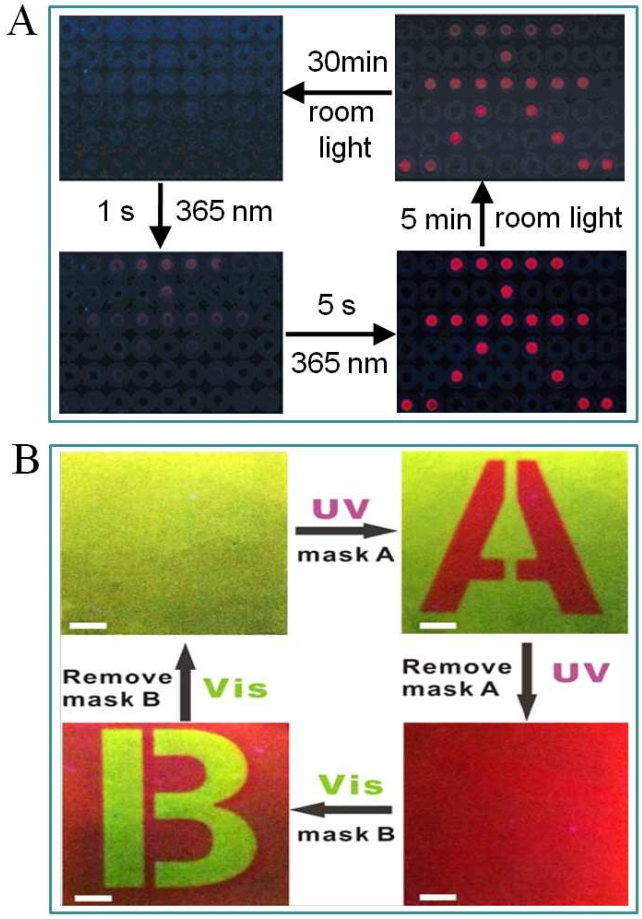

Figure 15, Alternating UV and visible light either encodes or erases optical data via photorewritable fluorescence. (A) Red fluorescence of spotted pattern with photoswitchable fluorescent polymeric NPs can be switched "On (writing) "and "Off (erasing)" many times. (B) Upon illumination of alternating UV and visible light, information in different channel (in different color) can be encoded or erased in a reversible manner. Reprinted with permissions from ref 36 and 95. Copyright (2006, 2015) American Chemical Society.

4. Conclusions and future perspectives

The past decade has witnessed the great success of the photoswitching-enable fluorescence analysis techniques capable of defying the practical challenges that the real-world applications of fluorescence technologies generally encounter, such as

super-resolution imaging methods that circumvents the longstanding diffraction-limit barrier. The key enabling factor in these breakthroughs such as super-resolution imaging and anti-phase dual-color correlation imaging is the growing availability of dynamic contrast agents with fluorescence emission features, either intensity or color, that can be modulated by photonic stimuli. Although improved data-processing algorithms and optical equipment are also needed, fluorescent probes with optimized performance continue to be the key-enabling factor in the future development. In terms of the wavelength-dependent light penetration ability and UV-induced photodamage, photoswitchable fluorescent NPs with the activation, fluorescence excitation and emission all in the NIR region will be highly desirable. Photoswitchable fluorescent NPs with small physical size may be especially useful for minimizing the potential perturbation that the probes give rise to the target live systems, enabling high labeling density in the cases of detecting weak signals from complicated physiological environments and elucidating fine structures in complex biological specimens. For photoswitching-based FDI, amplification of the target signal scales linearly with both the oscillation amplitude and the number of modulated cycle; thus developing probes with high on-to-off switching ratio and improved photostability will be a direction for further development. For photoswitching-based super-resolution imaging such as PULSAR, the ultimate resolution is limited by the S/N ratio of probes and the dye density, indicating probes with enhanced brightness and labeling efficiency will allow imaging with improved resolution. Finally, new probes with improved brightness and optimized photoswitching behavior are anticipated to balance the intrinsic trade-off between temporal and spatial resolutions in super-resolution imaging.

Acknowledgements

This work was supported by National Natural Science Foundation of China (Grant Nos. 21173262 and 21373218,) the National Science Foundation (Grant Nos. CHE-0805547, CHE-1213358, and CHE-1212429), and the “Hundred-Talent Program” of CAS to ZT.

Biography

Yuanlin Zhang obtained his M.S. from Henan University, China in 2014. He is currently pursuing a PhD in physical chemistry at University of Chinese Academy of Sciences (UCAS). His research interest is design, synthesis of fluorescent materials and their biological applications.

Kaiquan Zhang obtained his B.Sc. from Sichuan University, China in 2014. He is currently a graduate student in Chemistry at UCAS. He focuses on photoactive materials and their biological applications.

Jie Wang received his B.Sc. from Wuhan University, China in 2013. He is currently working toward a PhD in physical chemistry at UCAS. He focuses on photoswitchable fluorescent materials and their applications in bioimaging.

Zhiyuan Tian graduated from Wuhan University, China with a B.Sc. in 1995 and received his Ph.D. degree in 2005 at the Institute of Chemistry, Chinese Academy of Sciences (CAS). He received his postdoctoral research trainings at Queen's University in Canada, Washington State University, University of Washington, and Clemson University from 2005 to 2010. In 2011, he joined UCAS as a professor of chemistry. His research interests include nanoscaled fluorescent tags and sensors and their biological applications.

Alexander D. Q. Li received his B.Sc. at Jilin University, and his Ph.D. from Northwestern University (Evanston, IL). After graduation, he went to Los Alamos National Laboratory (Los Alamos, NM) as a postdoctoral director fellow and later became a Technical Staff Member. In 2000, he joined the faculty at Washington State University (Pullman, WA) as an associate professor, and currently he is a full professor of chemistry and materials science at WSU. His research interests include macromolecular design and engineering, advanced materials synthesis, biofunctionality and nanotechnology integration, self-assembly, and supramolecular systems.

Reference

1 M. Fialkowski, K. J. M. Bishop, R. Klajn, S. K. Smoukov, C. J. Campbell, and B. A. Grzybowski, *J.*

Phys. Chem. B, 2006, **110**, 2482.

2 M. M. Russew and S. Hecht, *Adv. Mater.*, 2010, **22**, 3348.

3 R. Klajn, J. F. Stoddart, and B. A. Grzybowski, *Chem. Soc. Rev.*, 2010, **39**, 2203.

4 A. Grinthal and J. Aizenberg, *Chem. Soc. Rev.*, 2013, **42**, 7072.

5 C. Roche and V. Percec, *Isr. J. Chem.*, 2013, **53**, 30.

6 R. Klajn, *Chem. Soc. Rev.*, 2014, **43**, 148.

7 Z. Y. Tian, W. W. Wu, and A. D. Li, *Photoswitchable Nanoprobes for Biological Imaging Applications*, in *Trace Analysis with Nanomaterials.*, 2010, **Edited by David T. Pierce and Julia Xiaojun Zhao**.

8 M. Irie, *Chem. Rev.*, 2000, **100**, 1685.

9 R. Klajn, K. J. M. Bishop, M. Fialkowski, M. Paszewski, C. J. Campbell, T. P. Gray, and B. A. Grzybowski, *Science*, 2007, **316**, 261.

10 R. Klajn, K. J. M. Bishop, and B. A. Grzybowski, *Proc. Natl. Acad. Sci. U. S. A.*, 2007, **104**, 10305.

11 M. Yamada, M. Kondo, J. I. Mamiya, Y. L. Yu, M. Kinoshita, C. J. Barrett, and T. Ikeda, *Angew. Chem. Int. Ed.*, 2008, **47**, 4986.

12 R. Klajn, K. P. Browne, S. Soh, and B. A. Grzybowski, *Small*, 2010, **6**, 1385.

13 O. Chovnik, R. Balgley, J. R. Goldman, and R. Klajn, *J. Am. Chem. Soc.*, 2012, **134**, 19564.

14 S. Das, P. Ranjan, P. S. Maiti, G. Singh, G. Leitus, and R. Klajn, *Adv. Mater.*, 2013, **25**, 422.

15 W. Kuch, *Nat. Mater.*, 2003, **2**, 505.

16 S. M. Aldoshin, *J. Photochem. Photobiol. A Chem.*, 2008, **200**, 19.

17 Q. S. Wei and A. Wei, *Chem. Eur. J.*, 2011, **17**, 1080.

18 M. J. Rust, M. Bates, and X. W. Zhuang, *Nat. Meth.*, 2006, **3**, 793.

19 E. Betzig, G. H. Patterson, R. Sougrat, O. W. Lindwasser, S. Olenych, J. S. Bonifacino, M. W. Davidson, J. Lippincott-Schwartz, and H. F. Hess, *Science*, 2006, **313**, 1642.

20 S. T. Hess, T. P. K. Girirajan, and M. D. Mason, *Biophys. J.*, 2006, **91**, 4258.

21 A. Sharonov and R. M. Hochstrasser, *Proc. Natl. Acad. Sci. U. S. A.*, 2006, **103**, 18911.

22 D. H. Hu, Z. Y. Tian, W. W. Wu, W. Wan, and A. D. Q. Li, *J. Am. Chem. Soc.*, 2008, **130**, 15279.

23 Y. Wu, Y. S. Xie, Q. Zhang, H. Tian, W. H. Zhu, and A. D. Q. Li, *Angew. Chem. Int. Ed.*, 2014, **53**, 2090.

24 W. L. Li, C. H. Jiao, X. Li, Y. S. Xie, K. Nakatani, H. Tian, and W. H. Zhu, *Angew. Chem. Int. Ed.*, 2014,

53, 4603.

25 W. L. Li, X. Li, Y. S. Xie, Y. Wu, M. Q. Li, X. Y. Wu, W. H. Zhu, and H. Tian, *Sci. Rep.*, 2015, **5**, 9186

26 I. Yildiz, E. Deniz, and F. M. Raymo, *Chem. Soc. Rev.*, 2009, **38**, 1859.

27 Z. Y. Tian, W. W. Wu, and A. D. Q. Li, *Chemphyschem*, 2009, **10**, 2577.

28 J. J. Zhang, Q. Zou, and H. Tian, *Adv. Mater.*, 2013, **25**, 378.

29 Z. Y. Tian and A. D. Q. Li, *Acc. Chem. Res.*, 2013, **46**, 269.

30 J. Folling, S. Polyakova, V. Belov, A. van Blaaderen, M. L. Bossi, and S. W. Hell, *Small*, 2008, **4**, 134.

31 H. Y. Jung, S. You, C. Lee, S. You, and Y. Kim, *Chem. Commun.*, 2013, **49**, 7528.

32 F. May, M. Peter, A. Hutten, L. Prodi, and J. Mattay, *Chem. Eur. J.*, 2012, **18**, 814.

33 D. Genovese, M. Montalti, L. Prodi, E. Rampazzo, N. Zaccheroni, O. Tosic, K. Altenhoner, F. May, and J. Mattay, *Chem. Commun.*, 2011, **47**, 10975.

34 J. Jeong, E. Yun, Y. Choi, H. Y. Jung, S. J. Chung, N. W. Song, and B. H. Chung, *Chem. Commun.*, 2011, **47**, 10668.

35 V. C. Edelsztein, E. A. Jares-Erijman, K. Mullen, P. H. Di Chenna, and C. C. Spagnuolo, *J. Mater. Chem.*, 2012, **22**, 21857.

36 M. Q. Zhu, L. Y. Zhu, J. J. Han, W. W. Wu, J. K. Hurst, and A. D. Q. Li, *J. Am. Chem. Soc.*, 2006, **128**, 4303.

37 L. Y. Zhu, W. W. Wu, M. Q. Zhu, J. J. Han, J. K. Hurst, and A. D. Q. Li, *J. Am. Chem. Soc.*, 2007, **129**, 3524.

38 Z. Y. Tian, W. W. Wu, W. Wan, and A. D. Q. Li, *J. Am. Chem. Soc.*, 2009, **131**, 4245.

39 Y. Lv, H. Liu, B. M. Zhao, Z. Y. Tian, and A. D. Q. Li, *Isr. J. Chem.*, 2013, **53**, 294.

40 J. H. Su, J. Chen, F. Zeng, Q. M. Chen, S. Z. Wu, and Z. Tong, *Polym. Bull.*, 2008, **61**, 425.

41 J. Chen, F. Zeng, S. Z. Wu, Q. M. Chen, and Z. Tong, *Chem. Eur. J.*, 2008, **14**, 4851.

42 H. Furukawa, M. Misu, K. Ando, and H. Kawaguchi, *Macromol. Rapid Commun.*, 2008, **29**, 547.

43 Z. K. Hu, Q. Zhang, M. Z. Xue, Q. R. Sheng, and Y. G. Liu, *Opt. Mater.*, 2008, **30**, 851.

44 Z. Hu, Q. Zhang, M. Xue, Q. Sheng, and Y. G. Liu, *J. Phys. Chem. Solids*, 2008, **69**, 206.

45 J. Chen, P. S. Zhang, X. Y. Yu, X. F. Li, H. W. Tao, and P. G. Yi, *J. Macromol. Sci. A*, 2011, **48**, 219.

46 J. Chen, P. S. Zhang, G. Fang, P. G. Yi, X. Y. Yu, X. F. Li, F. Zeng, and S. Z. Wu, *J. Phys. Chem. B*, 2011, **115**, 3354.

47 J. Chen, P. S. Zhang, G. Fang, P. G. Yi, F. Zeng, and S. Z. Wu, *J. Phys. Chem. B*, 2012, **116**, 4354.

48 I. Yildiz, S. Impellizzeri, E. Deniz, B. McCaughan, J. F. Callan, and F. M. Raymo, *J. Am. Chem. Soc.*, 2011, **133**, 871.

49 Y. Zou, T. Yi, S. Z. Xiao, F. Y. Li, C. Y. Li, X. Gao, J. C. Wu, M. X. Yu, and C. H. Huang, *J. Am. Chem. Soc.*, 2008, **130**, 15750.

50 M. Q. Zhu, G. F. Zhang, Z. Hu, M. P. Aldred, C. Li, W. L. Gong, T. Chen, Z. L. Huang, and S. Y. Liu, *Macromolecules*, 2014, **47**, 1543.

51 D. Tuncel and H. V. Demir, *Nanoscale*, 2010, **2**, 484.

52 Z. Y. Tian, J. B. Yu, C. F. Wu, C. Szymanski, and J. McNeill, *Nanoscale*, 2010, **2**, 1999.

53 A. Kaeser and A. P. H. J. Schenning, *Adv. Mater.*, 2010, **22**, 2985.

54 C. F. Wu and D. T. Chiu, *Angew. Chem. Int. Ed.*, 2013, **52**, 3086.

55 E. J. Harbron, C. M. Davis, J. K. Campbell, R. M. Allred, M. T. Kovary, and N. J. Economou, *J. Phys. Chem. C*, 2009, **113**, 13707.

56 C. M. Davis, E. S. Childress, and E. J. Harbron, *J. Phys. Chem. C*, 2011, **115**, 19065.

57 C. F. Chamberlayne, E. A. Lepekhina, B. D. Saar, K. A. Peth, J. T. Walk, and E. J. Harbron, *Langmuir*, 2014, **30**, 14658.

58 K. Jeong, S. Park, Y. D. Lee, C. K. Lim, J. Kim, B. H. Chung, I. C. Kwon, C. R. Park, and S. Kim, *Adv Mater.*, 2013, **25**, 5574.

59 Y. Kim, H. Y. Jung, Y. H. Choe, C. Lee, S. K. Ko, S. Koun, Y. Choi, B. H. Chung, B. C. Park, T. L. Huh, I. Shin, and E. Kim, *Angew. Chem. Int. Ed.*, 2012, **51**, 2878.

60 E. Petryayeva, W. R. Algar, and I. L. Medintz, *Appl. Spectrosc.*, 2013, **67**, 215.

61 V. Muhr, S. Wilhelm, T. Hirsch, and O. S. Wolfbeis, *Acc. Chem. Res.*, 2014, **47**, 3481.

62 D. M. Yang, P. A. Ma, Z. Y. Hou, Z. Y. Cheng, C. X. Li, and J. Lin, *Chem. Soc. Rev.*, 2015, **44**, 1416.

63 F. M. Raymo and M. Tomasulo, *Chem. Soc. Rev.*, 2005, **34**, 327.

64 I. L. Medintz, S. A. Trammell, H. Mattoussi, and J. M. Mauro, *J. Am. Chem. Soc.*, 2004, **126**, 30.

65 L. Y. Zhu, M. Q. Zhu, J. K. Hurst, and A. D. Q. Li, *J. Am. Chem. Soc.*, 2005, **127**, 8968.

66 E. Jares-Erijman, L. Giordano, C. Spagnuolo, K. Lidke, and T. M. Jovin, *Mol. Cryst. Liq. Cryst.*, 2005, **430**, 257.

67 M. Tomasulo, I. Yildiz, and F. M. Raymo, *Aust. J. Chem.*, 2006, **59**, 175.

68 W. H. Binder, R. Sachsenhofer, C. J. Straif, and R. Zirbs, *J. Mater. Chem.*, 2007, **17**, 2125.

69 S. A. Diaz, G. O. Menendez, M. H. Etchehon, L. Giordano, T. M. Jovin, and E. A. Jares-Erijman, *Acs*

Nano, 2011, **5**, 2795.

70 S. A. Diaz, L. Giordano, T. M. Jovin, and E. A. Jares-Erijman, *Nano Lett.*, 2012, **12**, 3537.

71 S. A. Diaz, L. Giordano, J. C. Azcarate, T. M. Jovin, and E. A. Jares-Erijman, *J. Am. Chem. Soc.*, 2013, **135**, 3208.

72 S. A. Diaz, F. Gillanders, E. A. Jares-ERijman, and T. M. Jovin, *Nat. Commun.*, 2015, **6:6036**, doi: 10.1038/ncomms7036 (2015).

73 J. C. Boyer, C. J. Carling, S. Y. Chua, D. Wilson, B. Johnsen, D. Baillie, and N. R. Branda, *Chem. Eur. J.*, 2012, **18**, 3122.

74 C. Zhang, C. H. Xu, L. D. Sun, C. H. Yan, *Chem-Asian J*, **2012**, 7, 2225.

75 M. Fernandez-Suarez and A. Y. Ting, *Nat. Rev. Mol. Cell Biol.*, 2008, **9**, 929.

76 M. Heilemann, P. Dedecker, J. Hofkens, and M. Sauer, *Laser Photonics Rev.*, 2009, **3**, 180.

77 B. Huang, M. Bates, and X. W. Zhuang, *Annu. Rev. Biochem.*, 2009, **78**, 993.

78 B. Huang, H. Babcock, and X. W. Zhuang, *Cell*, 2010, **143**, 1047.

79 M. Bates, B. Huang, M. J. Rust, G. T. Dempsey, W. Q. Wang, and X. W. Zhuang, *Single Molecule Spectroscopy in Chemistry, Physics and Biology*, 2010, **96**, 399.

80 Z. Y. Tian, A. D. Q. Li, and D. H. Hu, *Chem. Commun.*, 2011, 47, 1258.

81 A. D. Q. Li, C. L. Zhan, D. H. Hu, W. Wan, and J. N. Yao, *J. Am. Chem. Soc.*, 2011, 133, 7628.

82 W. Wan, M. Q. Zhu, Z. Y. Tian, and A. D. Q. Li, *J. Am. Chem. Soc.*, 2015, **137**, 4312.

83 J. C. Hsiang, A. E. Jablonski, and R. M. Dickson, *Acc. Chem. Res.*, 2014, **47**, 1545.

84 C. I. Richards, J. C. Hsiang, D. Senapati, S. Patel, J. H. Yu, T. Vosch, and R. M. Dickson, *J. Am. Chem. Soc.*, 2009, **131**, 4619.

85 C. I. Richards, J. C. Hsiang, A. M. Khalil, N. P. Hull, and R. M. Dickson, *J. Am. Chem. Soc.*, 2010, **132**, 6318.

86 C. Y. Fan, J. C. Hsiang, A. E. Jablonski, and R. M. Dickson, *Chem. Sci.*, 2011, **2**, 1080.

87 A. E. Jablonski, J. C. Hsiang, P. Bagchi, N. Hull, C. I. Richards, C. J. Fahrni, and R. M. Dickson, *J. Phys. Chem. Lett.*, 2012, **3**, 3585.

88 A. E. Jablonski, R. B. Vegh, J. C. Hsiang, B. Bommarius, Y. C. Chen, K. M. Solntsev, A. S. Bommarius, L. M. Tolbert, and R. M. Dickson, *J. Am. Chem. Soc.*, 2013, **135**, 16410.

89 Z. Y. Tian, W. W. Wu, W. Wan, and A. D. Q. Li, *J. Am. Chem. Soc.*, 2011, **133**, 16092.

90 M. Q. Zhu, G. F. Zhang, C. Li, M. P. Aldred, E. Chang, R. A. Drezek, and A. D. Q. Li, *J. Am. Chem. Soc.*,

2011, **133**, 365.

91 R. Y. Tsien, *Annu. Rev. Biochem.,* **1998**, 67, 509.

92 S. J. Lim, B. K. An, S. D. Jung, M. A. Chung, and S. Y. Park, *Angew. Chem. Int. Ed*., **2004**, 43, 6346.

93 V. Adam, H. Mizuno, A. Grichine, J. I. Hotta, Y. Yamagata, B. Moeyaert, G. U. Nienhaus, A. Miyawaki, D. Bourgeois, and J. Hofkens, *J. Biotechnol*., **2010**, 149, 289.

94 C. Li, H. Yan, L. X. Zhao, G. F. Zhang, Z. Hu, Z. L. Huang, M. Q. Zhu, *Nat. Commun.*, **2014**, 5:5709, doi: 10.1038/ncomms6709.

95 J. Chen, W. B. Zhong, Y. Tang, Z. Wu, Y. Li, P. G. Yi, J. H. Jiang, *Macromolecules*, **2015**, 48, 3500.

TOC

This review summarizes the recent advances in photoswitchable nanoparticles and their novel applications in super resolution imaging, frequency domain imaging, and anti-phase dual color correlation imaging.